Received: 26 September 2022 | Revised: 14 December 2022 | Accepted: 15 January 2023

DOI: 10.1002/mrm.29608

RESEARCH ARTICLE

Magnetic Resonance in Medicine

High-resolution motion- and phase-corrected functional MRI at 7 T using shuttered multishot echo-planar imaging

Saikat Sengupta[1,2] | **Avery Berman**[3,4] | **Jonathan R. Polimeni**[5,6,7] | **Kawin Setsompop**[8,9] | **William A. Grissom**[1,2,10]

[1]Vanderbilt University Institute of Imaging Science, Vanderbilt University, Nashville, Tennessee, USA

[2]Department of Radiology and Radiological Sciences, Vanderbilt University Medical Center, Nashville, Tennessee, USA

[3]Department of Physics, Carleton University, Ottawa, Ontario Canada

[4]University of Ottawa Institute of Mental Health Research, Ottawa, Ontario, Canada

[5]Athinoula A. Martinos Center for Biomedical Imaging, Massachusetts General Hospital, Charlestown, Massachusetts, USA

[6]Department of Radiology, Harvard Medical School, Boston, Massachusetts, USA

[7]Harvard-MIT Division of Health Sciences and Technology, Massachusetts Institute of Technology, Cambridge, Massachusetts, USA

[8]Radiology, Stanford University, Stanford, California, USA

[9]Electrical Engineering, Stanford University, Stanford, California, USA

[10]Biomedical Engineering, Vanderbilt University, Nashville, Tennessee, USA

Correspondence
William A. Grissom, Vanderbilt University Institute of Imaging Science, Vanderbilt University, 1161 21st Avenue South Medical Center North, AA-3114 Nashville, TN 37232-2310, USA.
Email: wgrissom@gmail.com

Funding information
National Institute of Biomedical Imaging and Bioengineering, Grant/Award Numbers: R01EB016695, U01EB025162, R01EB019437

Purpose: To achieve high-resolution multishot echo-planar imaging (EPI) for functional MRI (fMRI) with reduced sensitivity to in-plane motion and between-shot phase variations.

Methods: Two-dimensional radiofrequency pulses were incorporated in a multishot EPI sequence at 7T which selectively excited a set of in-plane bands (shutters) in the phase encoding direction, which moved between shots to cover the entire slice. A phase- and motion-corrected reconstruction was implemented for the acquisition. Brain imaging experiments were performed with instructed motion to evaluate image quality for conventional multishot and shuttered EPI. Temporal stability was assessed in three subjects by quantifying temporal SNR (tSNR) and artifact levels, and fMRI activation experiments using visual stimulation were performed to assess the strength and distribution of activation, using both conventional multishot and shuttered EPI.

Results: In the instructed motion experiment, ghosting was lower in shuttered EPI images without or with corrections and image quality metrics were improved with motion correction. tSNR was improved by phase correction in both conventional multishot and shuttered EPI and the acquisitions had similar tSNR without and with phase correction. However, while phase correction was necessary to maximize tSNR in conventional multishot EPI, it also increased intermittent ghosting, but did not increase intermittent ghosting in shuttered EPI. Phase correction increased activation strength in both conventional multishot and shuttered EPI, but caused increased spurious activation outside the brain and in frontal brain regions in conventional multishot EPI.

Conclusion: Shuttered EPI supports multishot segmented EPI acquisitions with lower sensitivity to artifacts from motion for high-resolution fMRI.

KEYWORDS
2D RF, BOLD, fMRI, GRAPPA, high spatial resolution, image reconstruction, multishot EPI, RF pulse design, segmented EPI, ultrahigh field

1 | INTRODUCTION

In recent years, considerable effort has been invested in increasing the spatial resolution of functional MRI (fMRI) scans,[1-3] motivated by the desire to resolve neural activity at submillimeter scales, across cortical layers and columns, and within subcortical and brainstem nuclei. A key limitation in achieving submillimeter resolution blood oxygen level dependent (BOLD) fMRI is that single-shot echo planar imaging, the workhorse of fMRI, is significantly constrained by the performance of current gradient hardware. The spatial encoding demands at submillimeter resolutions result in prohibitively long echo trains even with parallel imaging acceleration, necessitating long echo times and loss of BOLD sensitivity, severe geometric distortions, and increased T_2^* blurring. These issues become more challenging in view of the fact that signal-to-noise ratio (SNR) requirements generally necessitate the use of ultrahigh field (7T and higher) for submillimeter resolution fMRI, where off-resonance field distortions and T_2^* blurring are much more severe than at 3T.

Multishot or segmented EPI addresses these challenges by dividing the EPI readout trajectory into multiple acquisitions, each with their own excitation, which collect interleaved phase-encoded lines of k-space. This reduces the effective echo train length and echo spacing by the number of shots N_{shots}, which reduces sensitivity to off-resonance and geometric distortions, reduces T_2^* blurring, and enables shorter echo times, at the cost of increased scan time. However, multishot EPI is vulnerable to shot-to-shot phase variations that arise from motion, respiration and cardiac pulsation. Differences in these physiological states between the interleaved shots comprising an image's collected k-space data introduce phase inconsistencies in the data, which manifest as image ghosting and signal fluctuations in time series fMRI data that reduce sensitivity to neural activation. These artifacts are especially localized and intense for a small number of shots. Furthermore, shot-to-shot phase variations are amplified at ultrahigh field, making robust multishot high-resolution fMRI challenging. Their severity can be reduced by reducing the gap in time between collection of the shots by re-ordering each slice's shots to be collected consecutively rather than interleaved with the other slice's shots (i.e., loop over shots rather than slices at the inner-most sequence level) using the Fast Low-angle Excitation Echo-planar Technique,[4-6] but this does not completely alleviate the ghosting and creates a new challenge to stabilize signal amplitudes as the available longitudinal magnetization varies across shots.

In this work we describe a multishot "shuttered" EPI acquisition for high-resolution fMRI at 7T. Whereas a conventional multishot EPI sequence excites the entire slice prior to collecting each shot's k-space data, in shuttered EPI a multidimensional radiofrequency (RF) pulse is used to simultaneously perform slice selection and excite a set of shutters across the slice in the phase-encoded dimension. The shutters are moved between the shots to cover the entire slice. This enables an image to be reconstructed from each shot individually with (assuming ideal, nonoverlapping shutters) the same *g*-factor penalty within the excited shutter regions as an image reconstructed jointly from all the shots' data. This feature of shuttered EPI, which allows each individual shot to be reconstructed with less error compared to conventional multi-shot EPI, was leveraged in this work to reconstruct individual-shot images to estimate motion parameters, and then use those parameters to perform motion-corrected all-shots GRAPPA[7] reconstructions with much lower error than conventional multishot scans due to shuttered EPI's reduced coupling between shots in the reconstruction. Furthermore, as will be demonstrated, shuttered EPI has inherently reduced sensitivity to phase errors between shots, since phase differences only affect voxels in the overlapping regions between shutters. This feature was leveraged in this work to implement a simple shotwise phase correction within a GRAPPA reconstruction that increases temporal stability in voxels where the shutters overlapped, without increasing intermittent ghosting.

In the following we describe a multishot gradient-recalled echo shuttered EPI pulse sequence and a motion- and phase-compensated image reconstruction for a 7T implementation of the method. We then describe a set of in vivo experiments to evaluate shuttered EPI in the context of instructed in-plane motion, followed by an assessment of temporal stability and the method's application in a visual fMRI experiment with 0.8×0.8 mm^2 in-plane resolution. These studies will show that shuttered EPI enables improved in-plane motion compensation with less residual ghosting than conventional multishot EPI, that it achieves similar temporal signal-to-noise ratio (tSNR) with phase correction but with reduced intermittent ghosting artifacts, and that it has similar sensitivity to neural activity in a visual fMRI experiment but with less spurious activation outside the visual cortex. Due to a more complex excitation, these benefits currently come with the tradeoff of increased minimum slice thickness compared to conventional EPI, and potentially a smaller maximum number of slices per pulse repetition time (TR). Preliminary accounts of this work were reported at the ISMRM 2018[8] and 2022[9] meetings.

2 | THEORY

2.1 | Shuttered EPI 1/*g* and SNR

Figure 1A illustrates how shuttered EPI enables an image to be reconstructed from each shot individually with (assuming ideal, nonoverlapping shutters) the same 1/*g*-factor (which is proportional to SNR[10]) within the excited shutter regions as an image reconstructed jointly from all the shots' data. This is because, due to the controlled aliasing effect of the shuttered excitation, at each position within the shutters of a given shot only R pixels will alias with each other (where R is the parallel imaging acceleration factor), and by virtue of the spacing between shutters they will be separated by the same distance as in an all-shots reconstruction.[8,11,12] In contrast, each voxel of an image reconstructed from one shot of a conventional multishot scan will alias with $N_{shots} \times R$ others, yielding a much lower 1/*g*. Shuttered EPI does lose SNR by reduced signal averaging, but magnetization is also excited less frequently than in conventional multishot EPI, resulting in higher signal in each shuttered EPI shot as TR is decreased. A theoretic SNR analysis of shuttered versus conventional multishot EPI is provided in Figure S1 and associated text, which shows that overall, shuttered EPI comes with little SNR penalty and may increase SNR at short TRs and with more than four shots. Figure 1B shows example individual-shot-reconstructed shuttered images and a combined all-data shuttered image for $R = 4$ and $N_{shots} = 4$ at 7T, along with a conventional multishot EPI image acquired in the same slice location.

2.2 | Shuttered 2D RF Excitation Pulses

Figure 2A shows a 2D RF pulse for shuttered EPI. The pulse simultaneously selects a slice and a set of in-plane shutters, and is constructed following the method described in Reference 13 (section 5.1.1), wherein a small-tip-angle slice-selective RF pulse is first generated using the Shinnar Le-Roux algorithm. This pulse is replicated and each copy is weighted by its position in a spatially selective excitation envelope which is also generated by the Shinnar Le-Roux algorithm, with α polynomial phase cancellation[6] which leads to a slightly asymmetric pulse waveform but flatter excited phase across the shutters. This phase cancellation does not alter the pulse's isodelay, and the TE period starts halfway through the pulse. The design follows a bipolar (rather than flyback[11]) construction to minimize its duration. The area of the G_y

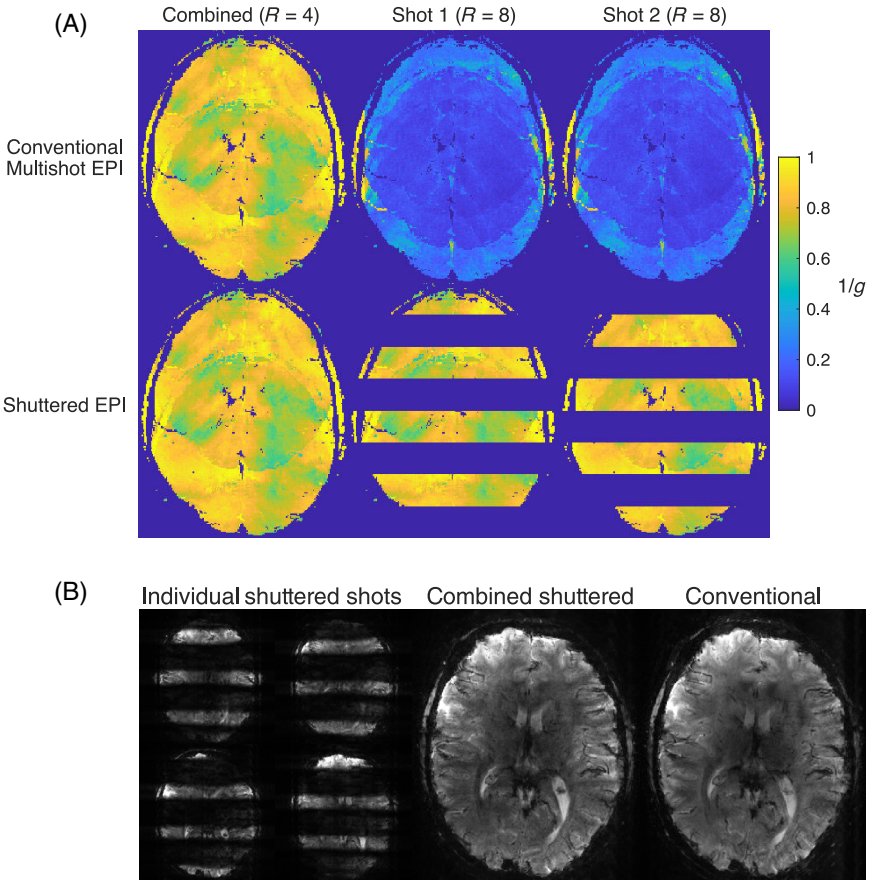

FIGURE 1 (A) 1/*g*-Factor maps of conventional and shuttered echo-planar imaging (EPI) scans for a two-shot, $R = 4$ acquisition with 32 coils. Instead of exciting the entire slice in each EPI shot/segment, a set of $R = 4$ equispaced shutters is excited in the EPI phase-encoded dimension using a multidimensional radiofrequency (RF) pulse, and the shutters are shifted between shots to cover the entire slice. An individual reconstruction from each shot's data yields an image within that shot's shutters with the same g-factor as an all-shots reconstruction, which can be used for motion and phase correction prior to the all-shots reconstruction. In contrast, reconstructions from a single shot's data in a conventional multishot EPI scan suffer much larger g-factor-related SNR losses. (B) Example individual-shot shuttered EPI images, a combined all-shots shuttered EPI image, and a conventional multishot EPI image acquired in the same prescribed slice location. These images are from subject C of the temporal stability and visual functional MRI experiments, with $N_{shots} = 4$ and $R = 4$.

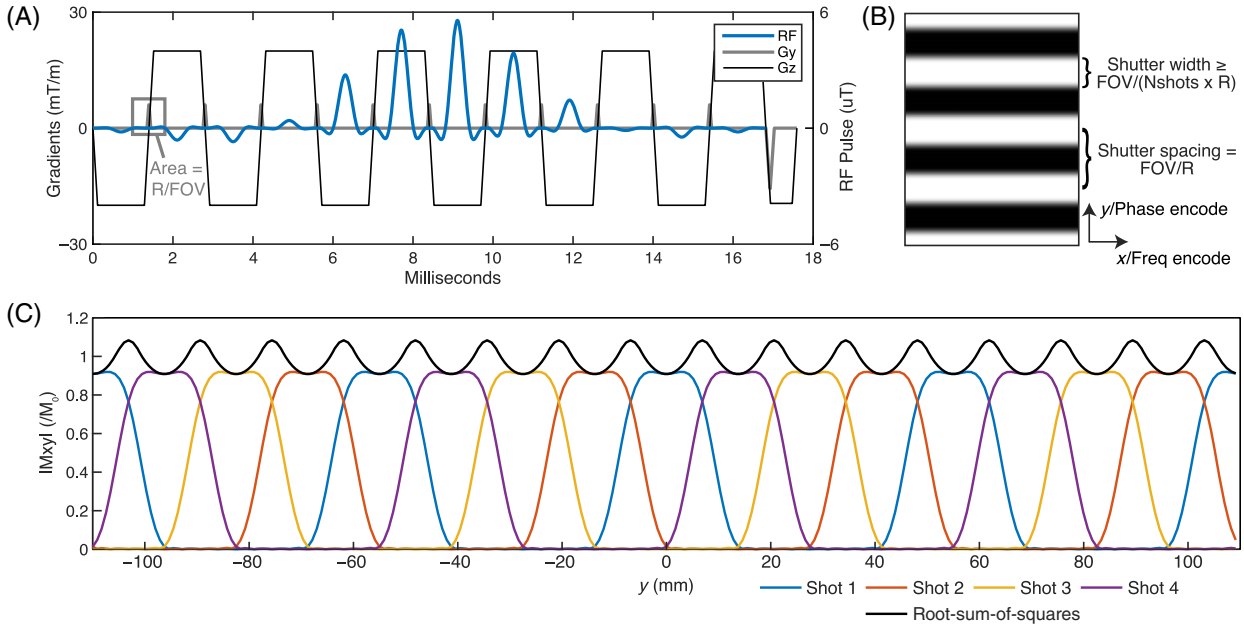

FIGURE 2 (A) The two-dimensional shutter excitation pulse used in the temporal stability and visual functional MRI experiments. It excites a 4 mm slice and a repeating pattern of 18.3 mm-wide shutters in the y dimension, for an $N_{\text{shots}} = 4$ acquisition with $R = 4$. (B) The geometry of a shuttered excitation. (C) Simulated shutter profiles excited by the pulse in (A), and their root-sum-of-squares combination.

phase encoding blips between the RF subpulses is set so that the excited shutters are field of view (FOV)/R apart; that is, the shutters are intentionally aliased across the imaged FOV, similar to power independent of the number of slices (PINS) pulses for multiband excitation for simultaneous multislice imaging.[14] If no overlap between the shutters is desired, their width will be FOV/($N_{\text{shots}} \times R$); as described below, in this work the shutter widths were increased to avoid low-signal bands between the shutters. Figure 2B illustrates the geometry of an excited shutter pattern and how it relates to FOV, R, and N_{shots}. To cover the entire imaged slice, the shutter patterns are shifted across the imaged FOV between shots by linearly incrementing the phase of the N_{sub} subpulses, according to:

$$\phi_{i,j} = \frac{2\pi i j}{N_{\text{shots}}}, \tag{1}$$

where $i \in 0, \ldots, N_{\text{shots}} - 1$ indexes shots and $j \in -N_{\text{sub}}/2, \ldots, N_{\text{sub}}/2 - 1$ indexes subpulses. Figure 2C plots all the profiles excited by the pulse in Figure 2A as they are shifted across the FOV between shots, and their root-sum-of-squares combination.

3 | METHODS

3.1 | Scanner and participants

All experiments were conducted on a 7 T Philips Achieva scanner (Philips Healthcare), with a single-channel birdcage transmit coil and a 32-channel receive array insert (Nova Medical). Four healthy adults volunteered to participate in the study (two females, ages 25–40). Prior to imaging, written informed consent was obtained from each participant in accordance with the Institutional Review Board at Vanderbilt University. One subject participated in the instructed motion imaging experiment, and the remaining three participated in the temporal stability and visual stimulation fMRI experiments.

3.2 | Shuttered 2D RF excitation pulses and multishot EPI pulse sequence

The pulse in Figure 2A was used in the temporal stability and visual stimulation fMRI experiments, and excited a 4 mm-thick slice using time-bandwidth product four slice-selective subpulses. The shutters were also designed with a time-bandwidth product four envelope and were designed to partially overlap between the four shots to avoid low-signal bands between the shutters, by setting the shutter width equal to the 220 mm-wide phase-encoded imaging FOV divided by ($N_{\text{shots}} - 1$)R, that is, the shutters were 220/12 = 18.3 mm wide with 4.55 mm overlap between adjacent shutters. The subpulse and envelope Shinnar Le-Roux designs all targeted 1% ripple levels in both pass and stop bands. Ramp sampling was not used and the pulse's gradient waveforms were designed for minimum duration subject to 20 mT/m maximum gradient amplitude and 200 mT/m/ms maximum gradient slew

rate. The pulse's total duration was 17.6 ms, comprising 12 1.4 ms-long subpulses and a 0.8 ms rewinder gradient. The instructed motion experiment used the same pulse shape but with phase-encoding blip areas set for that experiment's 228 mm phase-encoded FOV, four shots, and $R = 3$, that is, the shutters were 228/9 = 25.3 mm wide with 6.3 mm overlap between adjacent shutters. The use of bipolar slice-select gradients in the 2D RF pulses led to ghosted ($N/2$) excitations in the null regions between the shutters due to gradient delays and eddy currents, which was corrected using the method described in Appendix S1.

The shuttered excitation pulses were implemented in a standard interleaved multislice, multishot gradient-recalled echo EPI pulse sequence, with no other modifications. The sequence included echo-time shifting to reduce inter-segment discontinuities.[15] To match slice profiles, all full-FOV excitations used in the conventional multishot EPI scans in this work used the same slice-selective RF and gradient waveforms as the shuttered scans. Due to their matched flip angle but longer durations, the specific absorption rate (SAR) of the shuttered pulses was 3.5×-lower than the full-FOV excitation pulses, though SAR was not a limiting factor for either conventional multishot or shuttered EPI acquisitions. Image-based B_0 shimming was used in all experiments (MRCodeTool, Tesla Dynamic Coils).

3.3 | Image reconstruction

Raw data were exported from all experiments for offline image reconstruction in MATLAB R2021b (Mathworks). Image reconstruction started with conventional Nyquist ghost correction applied to each shot's data independently using no-blip one-dimensional navigator data acquired automatically at the beginning of each EPI scan.[16] All reconstructions (both individual-shot and all-shot) used GRAPPA, with a 3×4 kernel size (readout × phase-encode). Separate sets of GRAPPA kernels were fit for image reconstruction from individual shots for motion estimation, and for final image reconstruction from all shots jointly; that is, the all-shots reconstructions effectively used $N_{\text{shots}} \times N_{\text{coils}} = 128$ receiver channels. GRAPPA kernels were fit using fully sampled reference k-space data acquired immediately prior to each dynamic imaging run. To match TE and geometric distortions to the dynamic scans, the reference data were acquired with the same echo spacing, echo train length, and undersampling factor per shot; that is, for an N_{shots} dynamic scan with an acceleration factor of R, a fully sampled reference dataset comprised $N_{\text{shots}} \times R$ k-space segments. For shuttered EPI, fully sampled reference data were acquired for each shot's excitation pattern, but the excitations were interleaved in the same fashion as the dynamic scans for consistency of spin history and steady-state signal. To minimize the effects on the GRAPPA kernel fits of residual Nyquist errors and steady-state signal differences between reference and accelerated dynamic data which otherwise led to the appearance of dark bands between shutters, the auto-calibration signals (ACS) matrices for GRAPPA kernel fitting were constructed using only data from the phase encoding lines that would be acquired in the accelerated dynamic scans, and the target signal vectors were constructed using data from unacquired phase encoding lines. One additional correction (described in Appendix S1) was applied to the shuttered EPI reference data prior to their use in GRAPPA kernel fitting and motion and phase correction, to equalize signal amplitudes across each shot's reference k-space data as the signal approached steady state (no dummy acquisitions were used when collecting the reference data to minimize dummy scan time; five dummies of accelerated data were collected between the reference and dynamic scans). The GRAPPA kernels were fit using a Tikhonov-regularized pseudo-inverse of the ACS matrix, with a regularization parameter equal to $10^{-3}\sigma_{\max}^2$, where $\sigma_{\max}$ is the ACS matrix's largest singular value. Coil images were combined by root-sum-of-squares. We note that this reconstruction uses no explicit knowledge of the positions or shapes of the shutters; instead, within the reconstruction the shutter patterns effectively acted as additional shot-specific sensitivity patterns that multiplied into the receiver coil sensitivities.

Reconstruction of each time point's image started with individual-shot GRAPPA reconstruction and in-plane motion parameter estimation (rotation angle θ and translations (Δ^x, Δ^y)) which followed the algorithm illustrated in Figure 3. First, the shot's rotation angle was estimated by Fourier transforming (represented by the $G()$ operator in the figure which was implemented using a nonuniform FFT[17]) its image to k-space and calculating its correlation with a precalculated library of rotated reference images obtained from the fully sampled data acquired prior to each dynamic imaging run. The rotation angle with maximum correlation θ max was identified and the image was rotated by the negative of this angle to align with the reference image using a $G(-\theta_{\max})$ operator followed by inverse FFT. The rotated reference image library was calculated for angles between −10° and +10°, in steps of 0.125°. Following rotation correction, the shot's translation parameters were determined by FFT'ing its image and multiplying its Fourier transform into the complex conjugate of the (unrotated) reference image. The correlation between this product and a precalculated library of phase functions $e^{-\imath 2\pi(\Delta^x k_x + \Delta^y k_y)}$ was calculated and the displacements with maximum correlation were identified and used in the subsequent all-shots reconstruction. The phase function

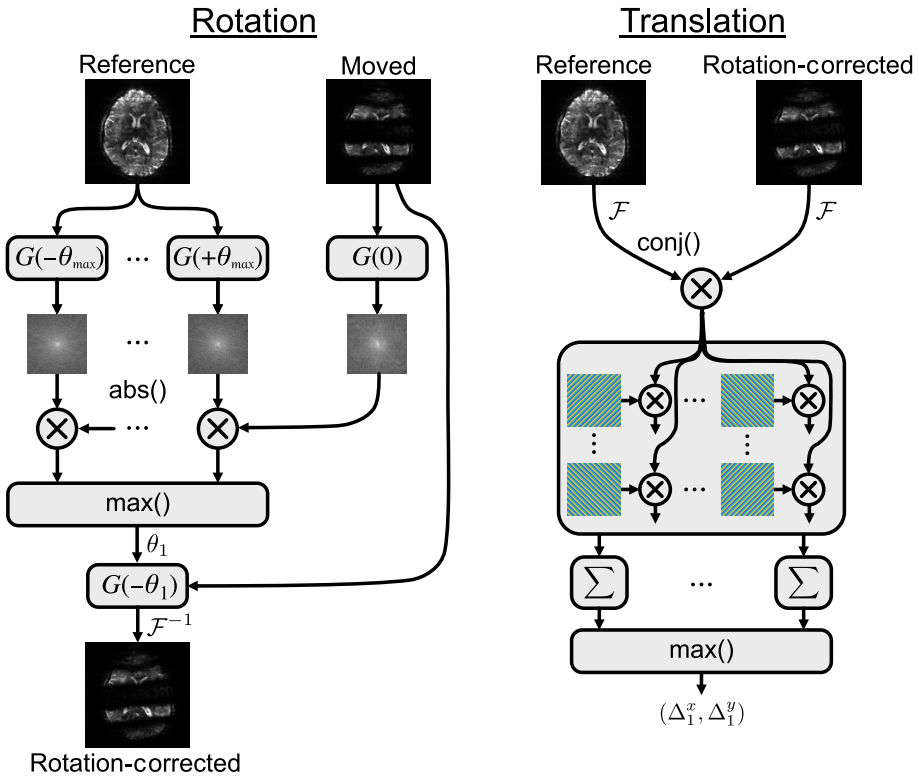

FIGURE 3 Motion estimation steps. Left: The rotation of each shot's image is estimated by transforming it to k-space, then calculating the correlations of its magnitude with the magnitudes of a library of rotated reference image k-spaces. The angle with maximum correlation is identified and rotation is corrected using a rotated Fourier Transform followed by inverse Fourier Transform. Right: The translation of each shot's rotation-corrected image is estimated by transforming it to k-space, then multiplying it by the complex conjugate of the reference image k-space, and correlating the result with a library of phase maps corresponding to translations in each image dimension. The translations with maximum correlation among these are identified as the translation between the reference and translated image. The parameters' "1" subscript is the shot's index.

library was calculated for displacements between −10 and +10 voxels, in steps of 0.125 voxels. We note that full-FOV reference images were used to determine motion parameters because the shutters did not move with the subject, so the use of corresponding individual shutter reference images would bias the motion parameters toward zero due to decreasing overlap between the reference and moved shutters with motion.

The final motion- and phase-corrected all-shot image reconstruction followed the algorithm illustrated in Figure 4. Based on the assumption that the coil sensitivities and the shutter patterns do not move with the head, GRAPPA predictions were first calculated from each shot's data (n is the shot index in the figure), yielding $N_{\text{shots}} \times N_{\text{coils}}$ filled k-space arrays, which were not summed with the other shots' predictions until after motion and phase correction. Motion correction was performed by inverse FFT of the filled k-spaces to the image domain, followed by multiplication with a $G(-\theta_n)$ operator that simultaneously corrected the shot's rotation and took the data back to k-space. Translations were corrected in k-space via multiplication with the phase function $e^{-\imath 2\pi\left(\Delta_n^x k_x + \Delta_n^y k_y\right)}$, yielding motion-corrected filled k-space arrays. To reduce shot-to-shot phase differences arising from motion and temporally varying B_0 inhomogeneity, a phase correction map was calculated by cropping the filled k-space data to the center 8×8 region, applying a Tukey window in that region, inverse Fourier transforming the cropped data to obtain low-resolution images, and multiplying the complex conjugates of those low-resolution images by corresponding low-resolution images obtained from retrospective undersampled GRAPPA reconstructions of the reference data, to obtain phase correction maps. The full-resolution filled k-space data was also inverse FFT'd and multiplied with the phase correction maps to obtain phase-corrected images for each coil and shot. Finally, the phase-corrected images were complex-summed with the corresponding images from the other shots, yielding $N_{\text{shots}} \times N_{\text{coils}}$ images that were combined by root-sum-of-squares to obtain the final combined image. This reconstruction was applied to both the shuttered EPI data and the conventional full-excitation multishot EPI data, with the same parameters.

3.4 | Experiments

3.4.1 | Instructed motion

To evaluate shuttered EPI's ability to compensate in-plane motion, an experiment was performed in which a subject was scanned with conventional multishot and shuttered EPI in three head positions: centered (the reference position for motion estimation), head rotated a medium angle clockwise, and head rotated a large angle counterclockwise. Scan parameters were: $N_{\text{shots}} = 4$, 228×228 mm^2 FOV, $1 \times 1 \times 4$ mm^3 voxels, 15 slices, $R = 3$, EPI echo train = 19, echo spacing = 1.74 ms (effective echo

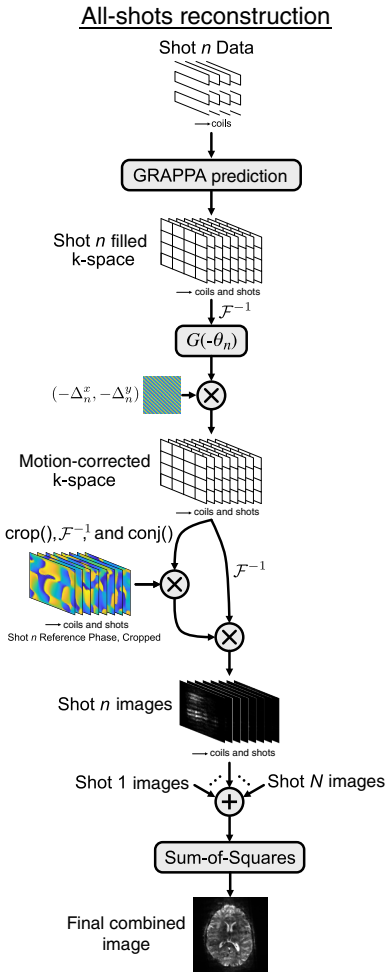

FIGURE 4 Image reconstruction steps. After the motion parameters are estimated, the final reconstruction proceeds by performing GRAPPA prediction for each shot individually, which yields filled k-spaces for all coils and shots, containing only the signal contributions from this shot. The data are inverse Fourier transformed and rotation and translation corrected, yielding motion-corrected k-space. The motion-corrected k-spaces are cropped and inverse Fourier transformed, and their phase difference with respect to reference images are calculated and subtracted from the inverse Fourier transform of the full k-spaces, yielding the final image signal contributions for this shot. These complex images are summed with the images produced by the other shots, and the final image is obtained by sum-of-squares.

spacing = 0.435 ms), TR/TE = 3000/27 ms, RF flip angle = 78° (both conventional and shuttered EPI). Fully sampled conventional and shuttered EPI reference data were acquired in each position, along with a single time point of accelerated data following five dummy acquisitions. GRAPPA kernels were trained using the centered reference position's reference data. By combining data in different positions, datasets were generated and reconstructed with between-scan motion (i.e. motion between the reference scan position and a dynamic position) and between-shot motion (i.e. motion between consecutive shots). Specifically, "between-scan" motion reconstructions used GRAPPA kernels and motion reference images obtained in the centered position to reconstruct dynamic images in the two rotated positions, while "between-shot" motion reconstructions used GRAPPA kernels and motion reference images obtained in the centered position to reconstruct dynamic images from data with interleaved centered and rotated shot data, that is, the dynamic image data comprised reference center position data for shot 1, rotated data for shot 2, reference center position data for shot 3, and rotated data for shot 4. Image reconstructions were performed with and without motion correction, and three quality metrics were calculated on the reconstructed images: normalized root-mean-square error (NRMSE) with respect to the reference position image, structural similarity index (SSIM) with respect to the reference position image, and root-mean-squared out-of-brain ghosted signal in an out-of-brain mask, normalized to RMS signal in the brain. All metrics were averaged across the 15 slices, and the NRMSE's and SSIM's were calculated after aligning the images to the reference position images, to measure image errors that could not be corrected by simple in-plane translations and rotations.

3.4.2 | Temporal stability and visual stimulation fMRI

Temporal stability and visual stimulation fMRI experiments were performed in the same scan sessions in three subjects. The scans used identical scan parameters: $N_{\text{shots}} = 4$, 220 × 220 mm^2 FOV, 0.8 × 0.8 × 4 mm^3 voxels, seven slices centered on the calcarine sulcus, $R = 4$, EPI echo train length = 17, echo spacing = 2 ms (effective echo spacing = 0.5 ms), TR/TE = 2000/28 ms, 150 dynamics/time points following five dummy acquisitions (total acquisition time of 310 s). Conventional scans used a 40° flip angle and shuttered scans used a 65° flip angle, which were determined to approximately maximize steady-state signal in gray matter.

Temporal stability is paramount to the detection of neural activation with fMRI and should be preserved or improved with the use of shuttered EPI. It was assessed by collecting data as described above with no stimulus (subjects at rest), reconstructing the time-series images, and calculating tSNR voxel-wise as the mean signal intensity over time (μ) divided by the SD over time (σ). To further characterize intermittent ghosting, voxel-wise temporal skewness was also calculated as:[6]

$$\text{skewness} = \frac{\left\langle (I(t) - \mu)^3 \right\rangle}{\sigma^3}, \quad (2)$$

where $I(t)$ is the signal intensity over time and $\langle\rangle$ denotes the temporal average. Skewness is sensitive to spurious departures from the expected signal intensity and is therefore well-suited to quantify intermittent ghosting. Finally, NRMSE versus the mean image across all time points was calculated. Conventional multishot and shuttered EPI images were reconstructed with no phase or motion correction, with phase correction only, and with both phase and motion correction, to evaluate the impact of the two corrections.

To demonstrate that shuttered EPI provides sufficient sensitivity and stability to detect functional responses with high in-plane spatial resolution while better localizing those responses, BOLD-weighted fMRI responses to a visual stimulus were measured in each subject. The stimulus was a standard 12 Hz black-and-white flickering "dartboard" pattern presented for 300 s in 10 8 s on/18 s off blocks with a neutral gray screen displayed during the off periods and 20 s pre- and post-stimulus periods. The stimulus was projected on an in-bore screen and viewed by a mirror inside the coil. Statistical activation maps from each run were computed independently with FSL FEAT.[18] No spatial smoothing nor prewhitening were performed. The regressors consisted of the stimulus paradigm convolved with a double-gamma variate as the Hemodynamic Response Function, as well as its temporal derivative. z-Score maps were calculated and overlaid on mean time-series magnitude images.

4 | RESULTS

4.1 | Instructed motion

Figure S4 shows the 15-slice shuttered EPI reference volume which was well-centered. Figure 5A shows images of the fifth slice reconstructed from all the shots' data and from only shot 2's data in each position which had an effective acceleration factor of 12; the images illustrate the degree of rotation relative to the reference position and the appearance of the individual-shot images used to estimate motion parameters in conventional and shuttered

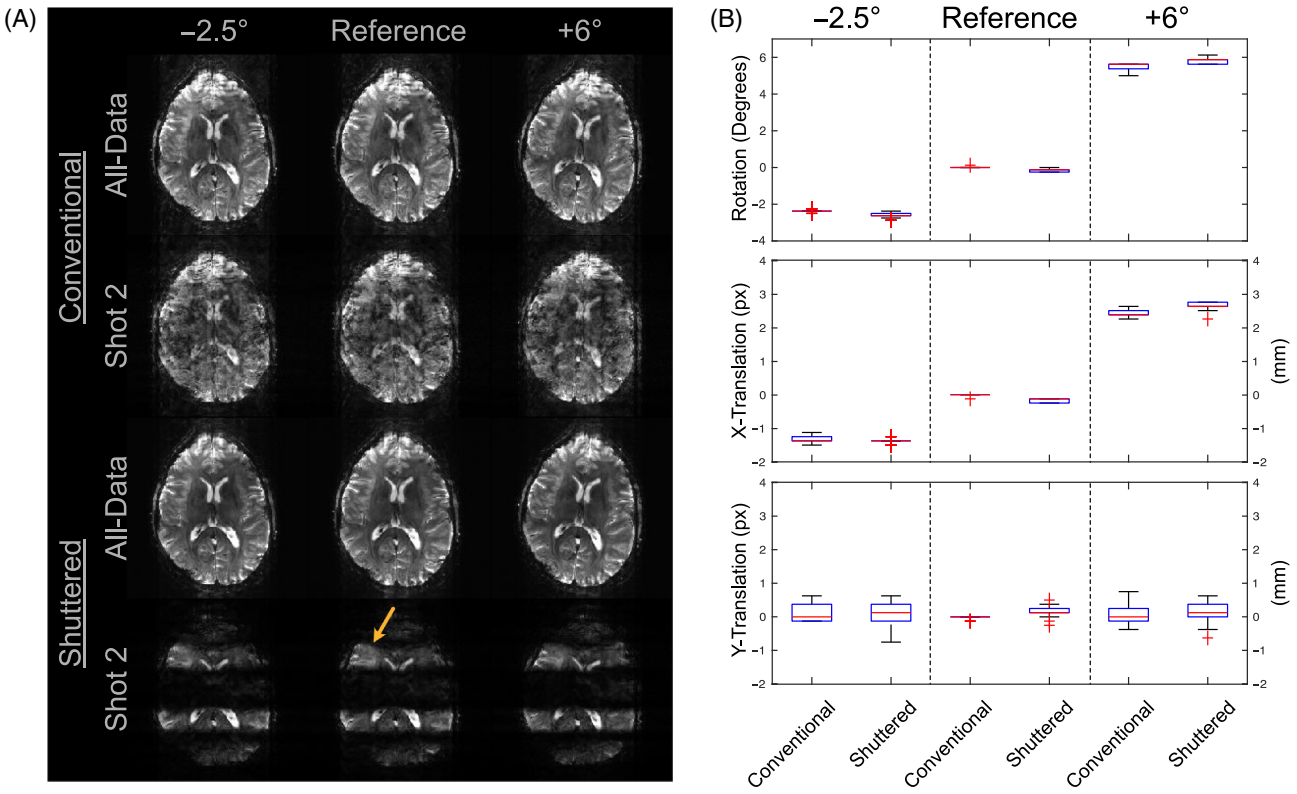

FIGURE 5 Motion images and estimated parameters. (A) Representative combined ("All-Data") and single-shot reference images for each position, for conventional and shuttered echo-planar imaging (EPI). In the −2.5° images the front of the head tilted left, and in the +6° images the head tilted right. The arrow indicates curving of a shutter due to off-resonance in the front of the brain. (B) Estimated motion parameters (rotation and translation in two dimensions), for each head position with respect to the reference position, across all slices and shots, for conventional and shuttered EPI. In each box, the central mark indicates the median across the 15 slices and four shots, and the bottom and top edges of the box indicate the 25th and 75th percentiles, respectively. The whiskers extend to the most extreme data points not considered outliers, and the outliers are plotted individually with the "+" marker.

EPI. The shot-2-only reconstruction with conventional full excitation contains aliasing and distortion throughout the slice, while the shuttered shot-2-only image shows good image quality within the shutter regions due to the lower *g*-factors there. The shutter images also demonstrate how the shutters do not move with the head motion, and how the shutters can shift due to off-resonance in frontal brain regions; with the pulses' 17.6 ms duration, the patterns shifted 0.096 mm per Hz off-resonance. The all-data images are nearly indistinguishable between conventional full-excitation and shuttered scans. Figure 5B plots the motion parameters (rotation (θ) and translation in two dimensions (Δ^x, Δ^y)) estimated from individual-shot reconstructions, across slices and shots, for conventional and shuttered EPI; the parameters were estimated with nearly the same mean and distribution in each position.

Figure 6A shows reconstructed images without and with motion correction for each motion configuration, and Figure 6B plots NRMSE, SSIM and out-of-brain ghosting across motion configurations, for conventional and shuttered EPI without and with motion correction. Even without motion correction, in most cases shuttered EPI had lower NRMSE, higher SSIM, and lower ghosting. These are reflected in the "No Moco" images in Figure 6A, in which ghosting is much higher in the conventional EPI images in all but the reference case, while shuttered EPI reconstructions reflect coherent motion, and in some cases coherent motion of individual features as indicated in the figure, but little other distortion. The much lower distortion in the shuttered EPI images is due to the lack of spatial overlap between the signals collected and reconstructed from each shot, which decouples the shots from each other in reconstruction except in overlapping regions, making the reconstruction less sensitive to motion between shots. In conventional multishot, each voxel's reconstructed signal strongly depends on all the shots' data, making it more sensitive to motion between the shots which is reflected in the larger image errors. Motion-corrected reconstruction reduced NRMSE, increased SSIM, and reduced ghosting in all cases, and motion-corrected shutter reconstructions had the lowest

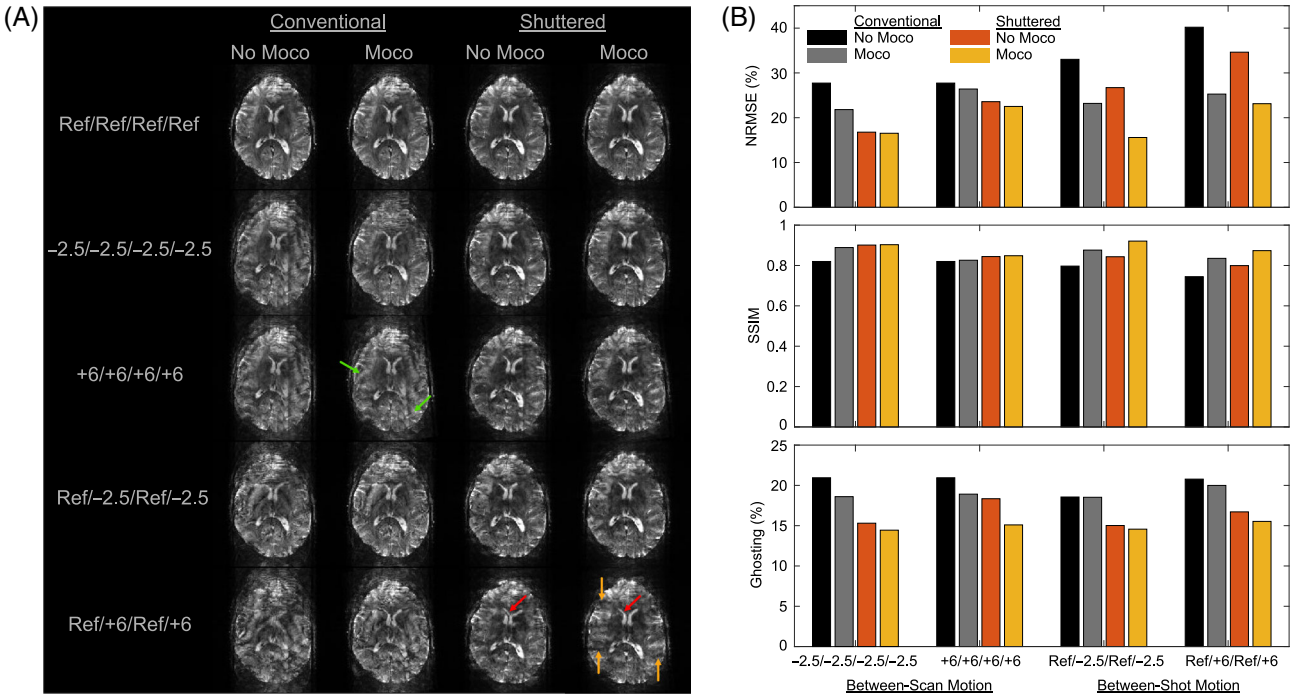

FIGURE 6 Motion-corrected image reconstruction results. Images were reconstructed with data combinations representing between-scan and between-shot motion, where the between-scan cases took all four shots' data from the −2.5° or +6° positions, and the between-shot cases interleaved the data of two shots from the reference position with two shots from the −2.5° or +6° positions. (A) Reconstructed images with and without motion correction, for conventional and shuttered echo-planar imaging (EPI) and each motion case. The green arrows point to within-brain ghosting in the conventional motion-corrected images, the red arrows point to a structure that is coherently shifted out of place in the uncorrected shutter image, but is correctly repositioned in the corrected shutter image, and the orange arrows point to dark bands that appear in the shuttered motion-corrected image due to gaps between adjacent shutters of the reference and +6° data. (B) Average image NRMSE, SSIM, and RMS out-of-brain ghosting (normalized to total brain signal), for each motion case with and without motion correction for conventional and shuttered EPI. The reference position out-of-brain ghosting was 13.7% for conventional EPI and 12.5% for shuttered EPI.

NRMSE, highest SSIM, and lowest ghosting. The reference position ghosting was 13.7% for conventional EPI and 12.5% for shuttered EPI; motion correction nearly restored the shuttered images to that level. The motion-corrected images in Figure 6A show that motion correction partially mitigated aliasing in the conventional EPI scans but did not completely suppress artifacts, while for shuttered EPI, motion correction mainly served to coherently shift the moved anatomy back to the reference position. However, as indicated in the figure very large motion between shots as in the interleaved reference/+6° case can lead to dark bands due to gaps between adjacent shutters.

4.2 | Temporal stability

Figure 7 shows tSNR maps in the middle slice for each subject with no correction, phase correction only, and phase and motion correction. The tSNRs of both conventional and shuttered EPI benefited considerably from phase correction in all three subjects: the maps show that tSNR is more uniform and higher with phase correction in all cases. In particular in the shuttered EPI case, phase correction increased tSNR in the overlapping regions between shutters, where phase differences between shots can cause signal cancellation. The plots in the top row of Figure 9 further show that without phase correction, shuttered EPI tSNR averaged over space was slightly higher than conventional EPI tSNR (average of 14.9 across subjects vs. 13.1) but that the tSNR of both methods increased significantly and were similar with phase correction in all subjects and were more similar on average (18.8 for shuttered EPI vs. 18.4 for conventional EPI). Due to relatively little motion in these scans (motion parameters are plotted in Figure S5), motion correction did not significantly increase or decrease tSNR in any case.

Figure 8 shows skewness maps in the middle slice for each subject with no correction, phase correction only, and phase and motion correction. Without phase correction, these images and the mean absolute skewness plots in Figure 9 show that conventional and shuttered EPI had similar skewness levels (0.20 for conventional versus 0.19 for shuttered EPI, averaged across subjects). However, they show that while phase correction increased tSNR for conventional multishot EPI, it also increased intermittent artifact levels and consequently skewness in all subjects but especially in the first two (subject-averaged mean absolute skewness = 0.29), but it did not consistently affect the shuttered EPI skewness (subject-averaged mean absolute skewness = 0.19). Figures S6–S8 show magnitude images, tSNR maps, and skewness maps across all slices for the three subjects, which confirm that the characteristics of the middle slice extend to the entire scan volumes.

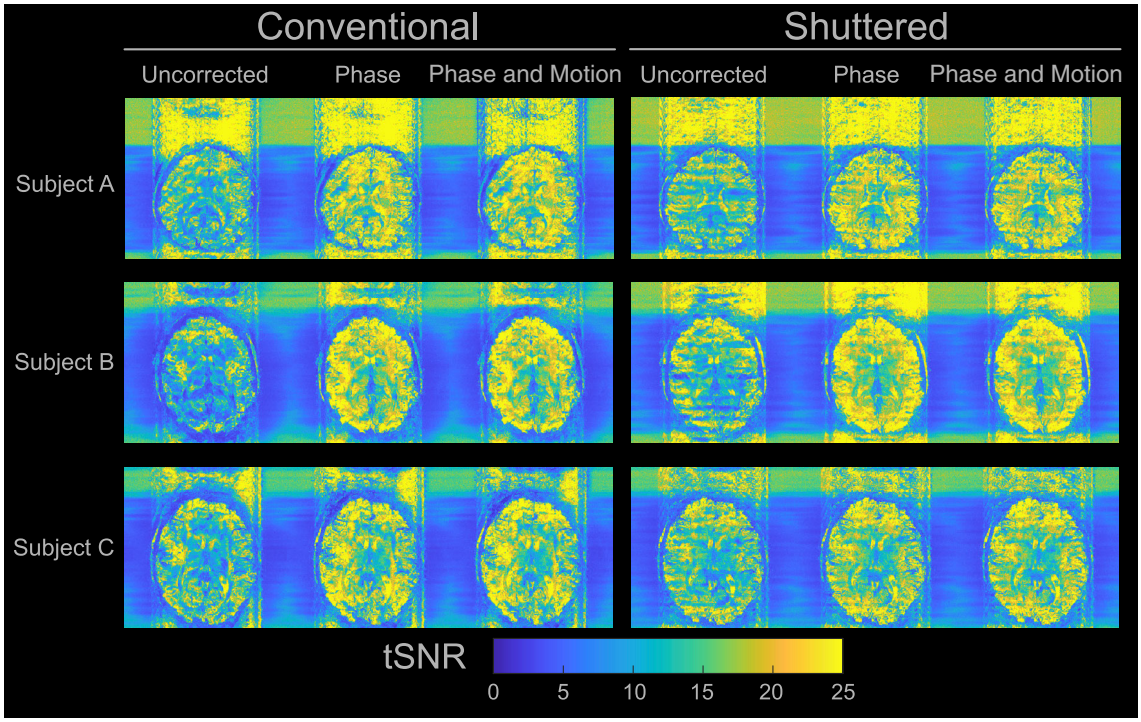

FIGURE 7 Temporal SNR (tSNR) maps of the middle slice of each subject's temporal stability scan. In all cases, phase correction led to higher and more spatially uniform tSNR. Further motion correction did not further observably affect tSNR.

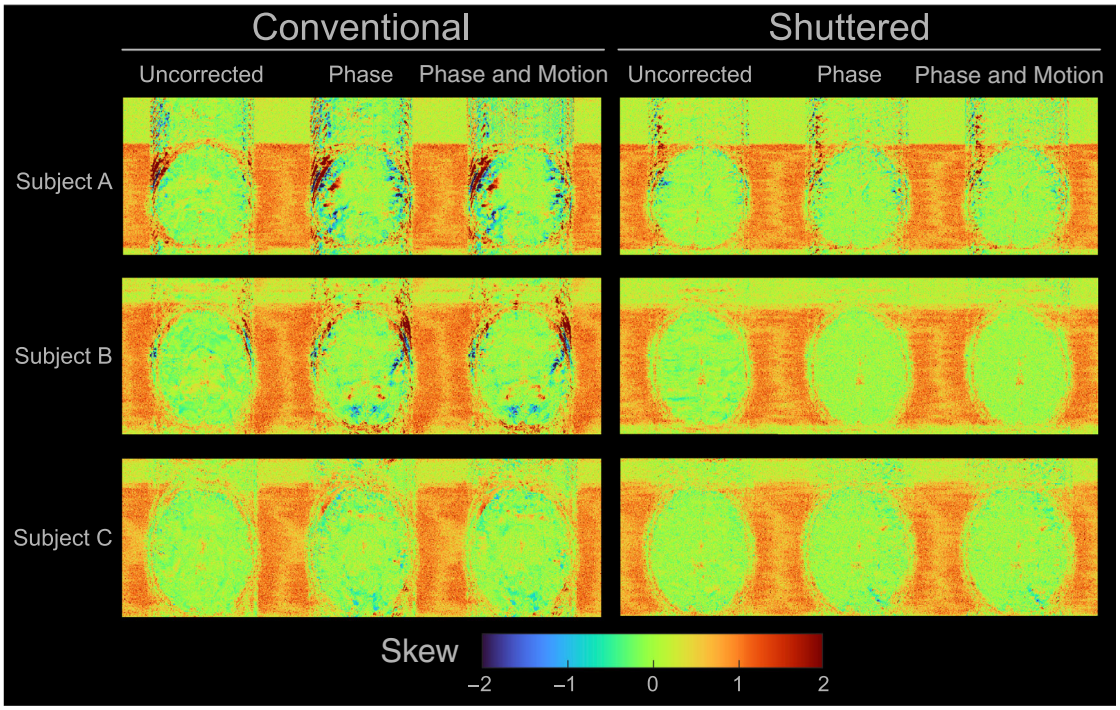

FIGURE 8 Skew maps of the middle slice of each subject's temporal stability scan. Phase correction led to higher skewness in all conventional scans, while it did not significantly affect skewness of the shuttered reconstructions. Further motion correction did not further significantly affect skewness in either case.

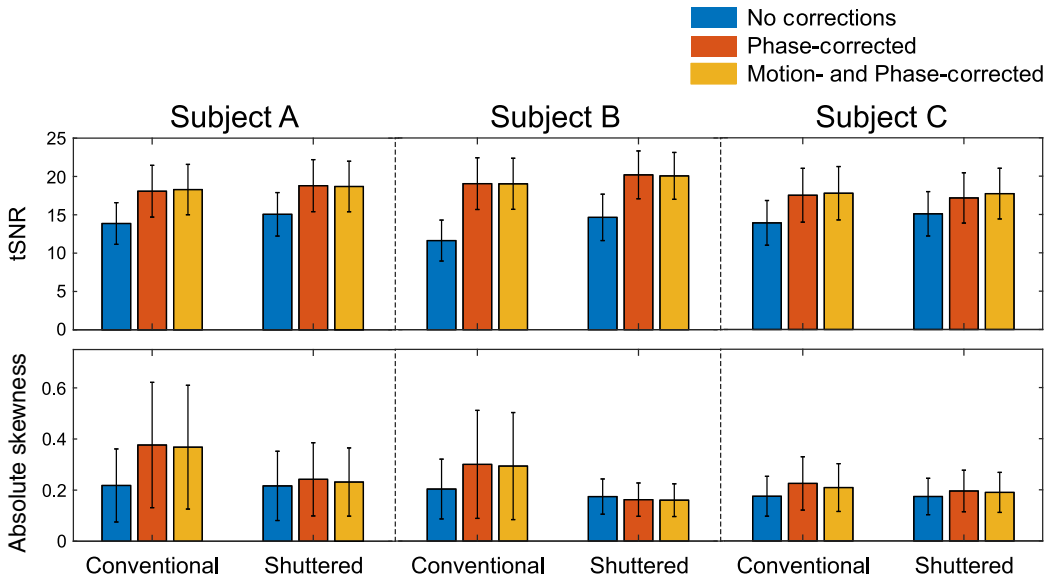

FIGURE 9 Spatial-average temporal SNR (tSNR) and absolute skewness across all slices of the temporal stability scans. The widths of the error bars indicate one SD. In each case the shuttered scans had higher mean tSNR without correction, and phase correction increased tSNR for both scans so that tSNRs were similar after correction. Motion correction did not significantly increase tSNR. However, phase correction did increase mean absolute skewness in the conventional case, indicating higher tSNR but also higher aliasing artfact levels in the conventional case. Phase correction did not significantly increase or decrease the skewness of shuttered echo-planar imaging images.

Figure S9 plots image NRMSE across time points referenced to time-series mean images for each subject's temporal stability scan, with and without phase and motion correction. The plots show that shuttered EPI's NRMSEs were generally lower without phase correction than conventional multishot EPI, and were further uniformly reduced by correction. Phase correction also almost always reduced NRMSE in conventional multishot EPI, but in each subject

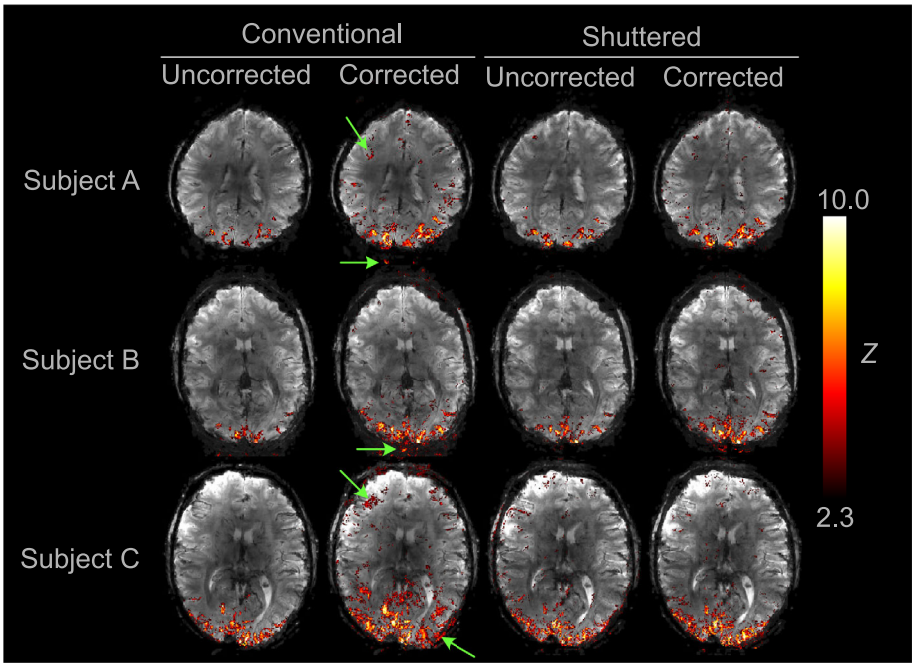

FIGURE 10 Activation maps in the middle slice of each subject's visual experiment. Phase and motion correction increased activation strength in both conventional and shuttered multishot echo-planar imaging, but also produced spurious activation in the front of and outside the brain in the conventional scans (green arrows)

it actually increased error for a handful of time points, likely due to a deep breath or out-of-plane motion; no sudden in-plane motion was detected at these time points. Videos S1–S3 show conventional and shuttered images of the middle slice without and with phase and motion correction at uniformly spaced time points through the scans, as well as their differences with the time-averaged image. The movies show that image differences in conventional EPI were relatively diffuse across the slice, while differences in shuttered EPI were more localized to the regions between shutters. Phase correction reduced differences in most regions throughout the slice in conventional EPI, but in some time points (the same time points with high NRMSE after phase correction) it increased differences in regions that coincided with the regions of elevated skewness in Figure 8.

4.3 | Visual stimulation fMRI

Figure 10 shows the results of the visual BOLD fMRI activation experiments, for conventional and shuttered multishot EPI without and with phase and motion correction. Responses are overlaid on the mean image from each run in the middle slice; all slices are shown for each subject in Figures S10–S12. Due to relatively little motion in these scans (motion parameters are plotted in Figure S13), motion-corrected reconstruction did not significantly increase or decrease activation in any case (results not shown). Without phase correction, shuttered EPI activations were stronger in all subjects than for conventional EPI (68.9% more voxels with $z > 2.3$), likely due to its higher tSNR at the back of the brain (Figure 7). Phase correction significantly increased the number and strength of activated voxels for both conventional and shuttered EPI, more so for conventional (263% more voxels with $z > 2.3$ with correction for conventional vs. 42.4% more voxels with $z > 2.3$ with correction for shuttered), however, it also led to a large number of activated voxels outside and in the front of the brain in the conventional EPI activation maps as indicated in the figure, whereas activations were better localized to the visual cortex in the shuttered EPI maps with motion and phase correction.

5 | DISCUSSION

5.1 | Overview

We have described a shuttered multishot EPI acquisition and reconstruction for high-resolution fMRI that uses 2D RF pulses to excite a set of bands or shutters across an imaged slice in a gradient-recalled echo scan, which are moved between shots to cover an imaged FOV. Results showed that the method has equivalent sensitivity (measured in terms of tSNR) compared to conventional multishot EPI, but reduced artifacts and image errors (measured in terms of skewness which is sensitive to spurious departures from expected signal intensity, ghosting outside the brain, and image NRMSE) and lower spurious activation in the presence of motion and phase variations between reference and dynamic scans, and also between shots. The similar tSNR after phase correction is consistent with the SNR calculations in Figure S1 which

predicted a 6% SNR loss for shuttered EPI with ideal non-overlapping shutters at 7T with the 2-s TR used here; this loss would be further reduced by the partial overlapping used in our scans which increases signal averaging in the overlapped regions. We also described a reconstruction pipeline including new approaches to phase and motion correction in EPI GRAPPA reconstruction, which are enabled by separately predicting each shot's filled k-space data, and determining and applying corrections to that data before summing with other shots' data to obtain the final filled k-space arrays. This reconstruction used no explicit information about the shapes or positions of the shuttered excitations and can be applied generally. In particular, the phase correction was shown to increase sensitivity to neural activation in both shuttered or conventional multishot EPI, in terms of both tSNR and number of activated voxels. However, for conventional EPI this increased sensitivity came at the cost of increased intermittent artifacts (measured in terms of skewness) and increased spurious activations distant from the expected visual cortex activations and also outside the brain, while skewness and artifactual activations did not increase significantly with phase correction in shuttered EPI. While the results in three subjects shown here were promising, further studies with more subjects should be performed to precisely measure the relative sensitivity and reliability of conventional multishot versus shuttered EPI in detecting functional activity. Overall, results indicated that the value of the shuttered EPI method for fMRI lies in its ability to reduce ghosting and other time-varying image artifacts, by limiting how far across the image the effects of motion and phase errors in individual shots shot can spread. Its benefits should increase with field strength as T_1 increases (which increases shuttered EPI's SNR relative to conventional multishot EPI) along with the severity of shot-to-shot phase variations (which increases the need for the robustness provided by shuttered EPI).

5.2 | Relation to other work

The present work is closely related to recent work in diffusion MRI. Specifically, Taviani et al.[12] proposed a multishot EPI 3T breast diffusion acquisition in which a 2D RF pulse was used to simultaneously excite a set of slices and a set of in-plane shutters along the EPI phase-encoded dimension. By moving the bands between EPI shots, signal was similarly collected across the entire phase-encoded FOV, and a full-FOV image could be reconstructed by treating the data from each shot as coming from a different set of receiver coils whose receive sensitivities were the product of the band pattern with the coil sensitivities. No further motion or explicit phase corrections were performed. The 2D RF pulse was designed to produce aliased slice excitations for additional acceleration via simultaneous multislice imaging, and the method was demonstrated in comparison to single-shot EPI, wherein it enabled increased resolution for a given echo train length, at the cost of N_{shots}-longer scan time. Later, Sun et al.[11] implemented this concept in diffusion imaging of the brain at 3T, using the same 2D RF pulse construction described in the present work. They similarly demonstrated the method's benefits in relation to single-shot EPI, mainly in reducing geometric distortions at the cost of increased scan time. Neither work compared the technique to conventional multishot EPI, where it may have been expected to reduce sensitivity to physiological phase variations and motion.

5.3 | Limitations

The main limitation of the current shuttered EPI technique is that while we achieved submillimeter in-plane resolution, we were limited to relatively thick slices (4 mm in this work). This was due to both the use of single-channel RF transmission, and to limited gradient performance on the scanner used in the study. Specifically, we found that gradient instabilities made it impossible to attenuate ghosted excitations between the shutters when running the gradient system at its full 40/200 capability, so we limited the gradient performance to 20/200, which led to relatively long 17.6 ms pulses. The pulse's long durations made the excited shutter patterns susceptible to blurring by in-plane off-resonance gradients, as could be appreciated in the frontal brain regions in individual-shot reconstructions in Figure 5. Since all the shot's pulses have matched durations and excitation k-space coverage, all the shutter patterns are blurred the same way, and because the reconstruction makes no assumptions on the specific shutter profile shapes, the method is not inherently "broken" by off-resonance. At the same time, if a large off-resonance gradient causes one shot's shutter to widen considerably while its neighbor's shutters narrow, then the effective reconstruction FOV of the shot with the wider band will increase, potentially leading to increased g-factor-related SNR losses. With commonly available 40/200 gradient performance, the pulse duration could have been shortened to 12.5 ms, almost 1/3 shorter. Conversely, the slice thickness could have been reduced by a similar proportion while maintaining the same pulse duration. The use of a minimum- or maximum-phase shutter envelope could also reduce the pulse duration another 10%–15%, with the tradeoff of a modest nonlinear residual phase across the shutters.[19] Another consideration is that the longer duration of shuttered pulses could limit the maximum number of imaged slices per TR, though this may be mitigated using a pulse design strategy that enables flexible setting of the pulses' isodelay, to make best use of dead time in the

pulse sequence.[20] Specific absorption rate was not a limitation in the present study, but could become a limitation as the pulse durations are decreased with stronger gradients to achieve shorter durations or to decrease slice thickness, or when shuttered EPI is combined with simultaneous multislice imaging. Ultimately, submillimeter slice thickness is desired for high-resolution fMRI, which ongoing and future work will address through the development of parallel transmission-enabled shuttered excitations,[21,22] and which also could be enabled by emerging gradient systems capable of up to much higher performance than 40/200.[23,24]

6 | CONCLUSION

Shuttered EPI is a multishot EPI technique that uses 2D RF pulses to excite a set of shutters across an imaged slice, which are moved between shots to cover the entire slice. It enables high-quality reconstruction of shuttered images from each individual shot which may be used for motion and phase correction, and it is less sensitive to phase variations between shots than conventional multishot EPI. At 7T it preserves the tSNR of multishot EPI with less intermittent ghosting. The tradeoff is an increased minimum slice thickness due to the need to simultaneously excite a slice and the shutter pattern with the sequence's excitation pulse.

FUNDING INFORMATION

This work was supported by NIH grants R01 EB016695, U01 EB025162, and R01 EB019437.

DATA AVAILABILITY STATEMENT

Code that implements the 2D RF pulse designs and image reconstructions performed in this study is available at https://github.com/grissomlab/shutteredEPI, including example data from this study.

ORCID

Saikat Sengupta https://orcid.org/0000-0001-5032-006X
Avery Berman https://orcid.org/0000-0001-7631-1049
William A. Grissom https://orcid.org/0000-0002-3289-1827

TWITTER

William A. Grissom @wgrissom

REFERENCES

1. DeMartino F, Yacoub E, Kemper V, et al. The impact of ultra-high field MRI on cognitive and computational neuroimaging. *NeuroImage*. 2018;168:366-382.
2. Dumoulin SO, Fracasso A, van der Zwaag W, Siero JCW, Petridou N. Ultra-high field MRI: advancing systems neuroscience towards mesoscopic human brain function. *NeuroImage*. 2018;168:345-357.
3. Bollmann S, Barth M. New acquisition techniques and their prospects for the achievable resolution of fMRI. *Progr Neurobiol*. 2021;207:101936.
4. Chapman B, Turner R, Ordidge RJ, et al. Real-time movie imaging from a single cardiac cycle by NMR. *Magn Reson Med*. 1987;5:246-254.
5. Polimeni JR, Bhat H, Witzel T, et al. Reducing sensitivity losses due to respiration and motion in accelerated echo planar imaging by reordering the autocalibration data acquisition. *Magn Reson Med*. 2016;75:665-679.
6. Berman AJL, Grissom WA, Witzel T, et al. Ultra-high spatial resolution BOLD fMRI in humans using combined segmented-accelerated VFA-FLEET with a recursive RF pulse design. *Magn Reson Med*. 2021;85:120-139.
7. Griswold MA, Jakob PM, Heidemann RM, et al. Generalized autocalibrating partially parallel acquisitions (GRAPPA). *Magn Reson Med*. 2002;47:1202-1210.
8. Sengupta S, Setsompop K, Grissom WA. Shuttered EPI brain imaging at 7 Tesla. *Proceedings 26th Scientific Meeting*. International Society for Magnetic Resonance in Medicine; 2018:216.
9. Sengupta S, Polimeni JR, Setsompop K, Grissom WA. Shuttered echo-planar fMRI with dynamic motion and phase correction. *Proceedings 30th Scientific Meeting*. International Society for Magnetic Resonance in Medicine; 2022:362.
10. Pruessmann KP, Weiger M, Scheidegger MB, Boesiger P. SENSE: Sensitivity encoding for fast MRI. *Magn Reson Med*. 1999;42:952-962.
11. Sun K, Zhong Z, Xu Z, Dan G, Karaman MM, Zhou XJ. In-plane simultaneous multisegment imaging using a 2D RF pulse. *Magn Reson Med*. 2022;87:263-271.
12. Taviani V, Alley MT, Banerjee S, et al. High-resolution diffusion-weighted imaging of the breast with multiband 2D radiofrequency pulses and a generalized parallel imaging reconstruction. *Magn Reson Med*. 2017;77:209-220.
13. Bernstein MA, Zhou XJ, King KF. *Handbook of MRI Pulse sequences*. 1st ed. Elsevier; 2004.
14. Norris DG, Koopmans PJ, Boyacioglu R, Barth M. Power independent of number of slices (PINS) radiofrequency pulses for low-power simultaneous multislice excitation. *Magn Reson Med*. 2011;66:1234-1240.
15. Feinberg DA, Oshio K. Phase errors in multi-shot echo planar imaging. *Magn Reson Med*. 1994;32:535-539.
16. Buonocore MH, Gao L. Ghost artifact reduction for echo planar imaging using image phase correction. *Magn Reson Med*. 1997;38:89-100.
17. Fessler JA, Sutton BP. Nonuniform fast Fourier transforms using min-max interpolation. *IEEE Trans Signal Process*. 2003;51:560-574.
18. Woolrich MW, Ripley BD, Brady M, Smith SM. Temporal autocorrelation in univariate linear modeling. *NeuroImage*. 2001;14:1370-1386.
19. Pauly JM, LeRoux P, Nishimura DG, Macovski A. Parameter relations for the Shinnar-Le Roux selective excitation pulse design algorithm. *IEEE Trans Med Imag*. 1991;10:53-65.
20. Grissom WA, Kerr AB, Holbrook AB, Pauly JM, ButtsPauly K. Maximum linear-phase spectral-spatial radiofrequency pulses

for fat-suppressed proton resonance frequency-shift MR thermometry. *Magn Reson Med*. 2009;62:1242-1250.
21. Cao Z, Yan X, Grissom WA. Parallel transmit excitation pulses for shuttered echo planar imaging. Paper presented at: Proceedings of International Society for Magnetic Resonance in Medicine; 2018; Paris, France: 386.
22. Cao Z. High resolution EPI with multi-spoke parallel transmission and virtual coil reconstruction. Paper presented at: Proceedings of International Society for Magnetic Resonance in Medicine; 2021; Virtual: 887.
23. Foo TKF, Tan ET, Vermilyea ME, et al. Highly efficient head-only magnetic field insert gradient coil for achieving simultaneous high gradient amplitude and slew rate at 3.0T (MAGNUS) for brain microstructure imaging. *Magn Reson Med*. 2020;83:2356-2369.
24. Feinberg D, Dietz P, Liu C, et al. Design and development of a next-generation 7T human brain scanner with high-performance gradient coil and dense RF arrays. Paper presented at: Proceedings of International Society for Magnetic Resonance in Medicine; 2021; Virtual: 562.

SUPPORTING INFORMATION

Additional supporting information may be found in the online version of the article at the publisher's website.

APPENDIX S1. Supporting information

VIDEO S1. Subject A

VIDEO S2. Subject B

VIDEO S3. Subject C

How to cite this article: Sengupta S, Berman A, Polimeni JR, Setsompop K, Grissom WA. High-resolution motion- and phase-corrected functional MRI at 7 T using shuttered multishot echo-planar imaging. *Magn Reson Med*. 2023;1-15. doi: 10.1002/mrm.29608